Supplementary Information

Flowable Organic Slurry Battery with 1000 Cycles

Rajeev K. Gautam, Xiao Wang, Amir Lashgari, Jianbing "Jimmy" Jiang*

Department of Chemistry, University of Cincinnati, P.O. Box 210172, Cincinnati, Ohio 45221,

United States

*Corresponding author: Email: jianbing.jiang@uc.edu

Table of Contents

Experimental Section

General methods. All chemicals were purchased from Sigma-Aldrich, Alfa Aesar, or Thermo Fisher Scientific. Other commercial solvents and reagents were used without further purification. DI water was used in all experiments.

Physical characterizations. FEI Apreo SEM was used to characterize the surface morphology of slurries before and after battery cycling. All slurry samples were placed on double-sided carbon tape and then the surface morphologies were captured in an energy X-ray spectroscopy mode. Further, EDS was used to examine the slurry samples' distribution of C, N, and O elements.

Electrochemical characterizations. Cyclic voltammetry (CV) and electrochemical impedance spectroscopy (EIS) were analyzed using a Bio-Logic potentiostat. A three-electrode system consisting of a slurry-coated glassy carbon as the working electrode, Ag/AgCl as the reference electrode, and platinum wire as a counter electrode in 0.1 M KCl aqueous solution was used to perform CV experiments. The aqueous slurry of **C18-V** was directly placed on the surface of a glassy carbon electrode to investigate its redox-active behavior. EIS experiments on all the slurry batteries were conducted over the frequency range of 100 kHz to 10 mHz.

Battery performance measurements. The half-slurry/half-flow battery setup was fabricated using a polytetrafluoroethylene plate, copper plate, graphite plate, silicone gasket, and graphite felt electrodes with an active area of 1.0 cm^2. The Fumasep cation exchange membrane was sandwiched between graphite felt electrode and slurry. For the aqueous catholyte, 0.2 M $K_4Fe(CN)_6$ and 0.1 M $K_3Fe(CN)_6$ were dissolved in 15 mL H_2O/TEGDME (95/5, v/v) with 0.5 M KCl. The TEGDME (5 wt.%) was used as an additive to enhance the stability of the aqueous solution. A peristaltic pump was employed to circulate the $K_4Fe(CN)_6/K_3Fe(CN)_6$ catholyte through the carbon felt electrode at a flow rate of 30 mL min^{-1}. The slurry analytes were prepared

in the aqueous solution of 1.0 M KCl in H_2O/TEGDME (95/5, v/v), where TEGDME was used as the surfactant.

The mass fraction of **Cn-V** was obtained from the mass of the whole slurry. The battery was galvanostatically charged/discharged in the voltage range of 0–1.6 V. In the first 20 cycles of the long-cycling study, the battery was tested under galvanostatic and potentiostatic charging/discharging conditions. The rate performance of the battery was reported for an average of 5 cycles at different current densities. The impedance of the battery was conducted via EIS with a frequency ranging from 200 kHz to 100 MHz.

Synthesis of Cn-V (n = 8, 12, 18) compounds

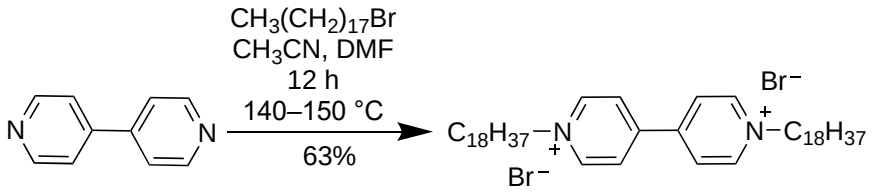

C18-V

Synthesis of C18-V. A sample of 1-bromooctadecane (10.7 g, 32.0 mmol, 4.00 eq) in DMF (30 mL) was added to the solution of 4,4'-dipyridyl (1.25 g, 8.00 mmol, 1.00 eq) in CH_3CN (8 mL) and stirred for 12 hours at 150 ºC. After cooling down the solution to room temperature, the crude mixture was centrifuged and washed twice with CH_3CN and hexenes to remove unreacted starting materials. The residue was dried under vacuum to afford **C18-V** as a yellow-white solid. Yield: 4.15 g, 63%. HR-MS: obsd 331.3233, calcd 331.3234 ([M^{2+}], M = $C_{46}H_{82}N_2$). ^{1}H NMR (400 MHz, DMSO-d_6), δ 0.85 (t, 6H, *J* = 8.0 Hz), 1.08–1.37 (m, 60H), 1.85–2.05 (m, 4H), 4.67 (t, 4H, *J* = 8.0 Hz), 8.78 (d, 4H, *J* = 8.0 Hz), 9.38 (d, 4H, *J* = 8.0 Hz). (^{13}C NMR did not show any signal due to very low solubility of **C18-V**.)

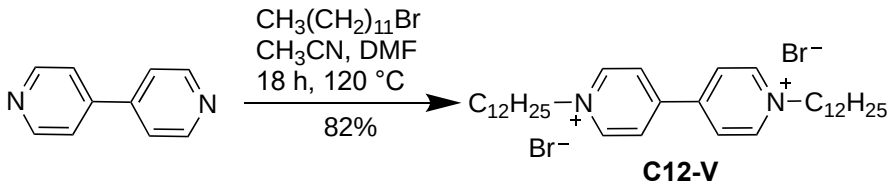

Synthesis of C12-V. A sample of 1-bromododecane (5.98 g, 24.0 mmol, 3.00 eq) in DMF (25 mL) was added to the solution of 4,4'-dipyridyl (1.25 g, 8.0 mmol, 1.00 eq) in CH_3CN (8 mL) and stirred for 18 hours at 120 ºC. After cooling down the solution to room temperature, the crude mixture was centrifuged and washed twice with CH_3CN and hexenes to remove unreacted starting materials. The precipitate was dried under vacuum to afford **C12-V** as a yellow solid. Yield: 4.27 g, 82%. HR-MS: obsd 247.2293, calcd 247.2294 ([M^{2+}], M = $C_{34}H_{58}N_2$). ^{1}H NMR (400 MHz, DMSO-d_6), δ 0.78–0.92 (m, 6H), 1.16–1.39 (m, 36H), 1.90–2.07 (m, 4H), 4.69 (t, 4H, *J* = 8.0 Hz), 8.80 (d, 4H, *J* = 8.0 Hz), 9.41 (d, 4H, *J* = 8.0 Hz); ^{13}C NMR (100 MHz, DMSO-d_6), δ 13.89, 22.03, 25.41, 28.37, 28.91, 30.67, 31.26, 60.91, 126.56145.75.

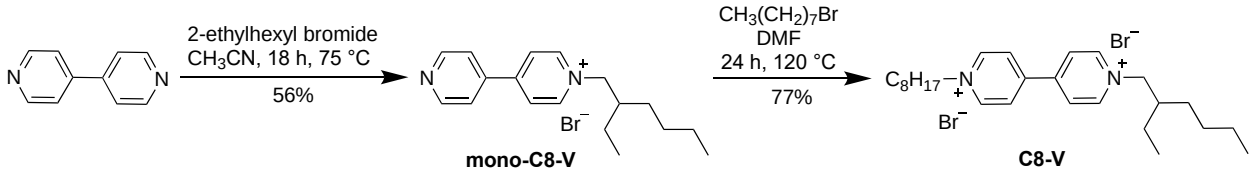

Synthesis of C8-V. A sample of 2-ethylhexyl bromide (4.64 g, 24.0 mmol, 3.00 eq) was added to the solution of 4,4'-dipyridyl (1.25 g, 8.0 mmol, 1.00 eq) in CH_3CN (10 mL) and stirred for 18 hours at 75 ºC. After cooling down the solution to room temperature, the crude mixture was centrifuged and washed twice with CH_3CN and hexenes to remove unreacted starting materials. The precipitate was dried under vacuum to afford **mono-C8-V** as a pale yellow solid. **mono-C8-V**: Yield: 1.56 g, 56%. ^{1}H NMR (400 MHz, DMSO-d_6), δ 0.77–0.91 (m, 6H), 1.09–1.48 (m, 8H), 1.98–2.19 (m, 1H), 4.68 (d, 2H, *J* = 8.0 Hz), 8.42 (d, 2H, *J* = 8.0 Hz), 8.88 (d, 2H, *J* = 8.0 Hz), 9.08 (d, 2H, *J* = 8.0 Hz), 9.47 (d, 2H, *J* = 8.0 Hz)

To a sample of **mono-C8-V** (100 mg, 0.29 mmol, 1.00 eq) in DMF (25 mL), a sample of 1-bromooctane (168.00 mg, 0.87 mmol, 3.00 eq) was added and stirred for 24 hours at 120 ºC. After cooling to room temperature, the crude mixture was filtered and washed with hexenes. The solid was dissolved in MeOH and after filtration and removing the solvent, it was dried under vacuum to afford **C8-V** as a pale yellow solid. **C8-V**: Yield: 121 mg, 77%. HR-MS: obsd 381.3263, calcd 381.3264 ($[M–H]^+$, M = $C_{26}H_{41}N_2$). ^{1}H NMR (400 MHz, CD_3OD), δ 0.85–0.95 (m, 6H), 0.98 (t, 3H, *J* = 8.0 Hz), 1.26–1.52 (m, 18H), 2.05–2.22 (m, 3H), 4.73 (d, 2H, *J* = 8.0 Hz), 4.78–4.84 (m, 2H), 8.69–8.78 (m, 4H), 9.29 (t, 4H, *J* = 8.0 Hz); ^{13}C NMR (100 MHz, DMSO-d_6), δ 10.51, 14.30, 14.39, 23.67, 23.92, 24.06, 27.25, 29.28, 30.09, 30.19, 30.75, 30.59, 32.88, 35.47, 42.59, 63.29, 66.59, 128.41, 147.11, 147.42, 151.33.

Molecular designs

The molecular engineering of viologen compounds has been an extremely effective approach to suppress the viologen radical dimerization and impart solubility properties. Hence, modified viologen compounds, **Cn-V** (n = 8, 12, 18) were synthesized with suppressed solubility to develop high-energy-density slurry batteries. Compounds **C18-V**, **C12-V**, and **C8-V** with varying lengths of alkyl chains were synthesized by the alkylation of 4,4'-dipyridyl. To synthesize **C18-V** and **C12-V**, 4 and 3 equivalents of the corresponding alkyl bromide are required, respectively. Owing to the low solubility of the final products in acetonitrile and hexanes, starting materials were easily washed and filtered to afford the final products in high purity and yields. For the synthesis of **C8-V**, the simultaneous di-alkylation of 4,4'-dipyridine was unsuccessful. Alternatively, monoalkylation was first performed using three equivalents of 2-ethylhexyl bromide to afford **mono-C8-V**. The second alkylation with 2-ethylhexyl bromide was unsuccessful. However, the use of 1-bromooctane successfully yielded the asymmetric **C8-V** compound. Detailed procedures

for the synthesis of **Cn-V** compounds are provided in the supporting information. Compounds **C18-V** and **C12-V** were highly insoluble in both aqueous and non-aqueous media, while **C8-V** showed a solubility of up to ~0.6 M in aqueous and ~0.4 M in non-aqueous (dimethylformamide) electrolyte. Therefore, **C18-V** and **C12-V** were selected for the subsequent aqueous slurry battery studies.

Ketjen black (KB) optimization in Cn-V slurry

A uniform conducting network, the so-called percolating network within the aqueous slurry, is essential for efficient charge transfer during the charge/discharge processes of the battery. Ketjen black (KB) is a prime choice as an additive conductive material for such applications owing to its high electrical conductivity and highly porous structure. However, achieving an optimal dispersion of KB particles within the slurry is crucial for maximizing slurry battery performance. Therefore, the electroconductive slurry of **C18-V** or **C12-V** was prepared by adding different KB concentrations (100, 200, 240, and 300 g/L). Before adding supporting electrolytes, both Cn-V and KB were mixed rigorously to ensure uniform distribution of the conducting network of KB chains. The uniform distribution of slurry constituents (**Cn-V** and KB) ensures an efficient redox reaction along with the capacity utilization of viologen redox molecules. To optimize the loading of KB, different concentrations of KB (100, 200, 240, and 300 g/L) were fabricated in 1.0 M KCl in an H_2O/tetramethylene glycol dimethyl ether (TEGDME, 95:5, v:v) solution. TEGDME was used to achieve the high homogeneity of the KB in the slurry. The **C18-V** slurries with different concentrations of KB were applied on the glassy carbon electrode and screened through electrochemical impedance spectroscopy (EIS), as shown in Figure S1. EIS spectra (Figure S1A and S1B) indicate an insignificant variation in the solution resistance (R_s), while the charge transfer resistance (R_{ct}) varies significantly for different KB loading. A higher value of R_{ct} indicates poor

electrocatalytic behavior or high charge transport losses in the aqueous slurry. The slurry at the low KB loading of 100 g/L exhibits a high R_{ct} (25.3 Ω) owing to a poor conducting network formed by the low loading of KB particles. However, R_{ct} reduced from 25.3 Ω to 11.7 Ω with an increase in the KB concentrations from 100 g/L to 240 g/L, respectively, as higher KB loading promoted the formation of the network in the slurry owing to the improved connection between KB and **C18-V** molecules. The slurry with a KB concentration of 240 g/L exhibited the lowest value of R_{ct}, which ensures better distribution of conducting KB chains within the **C18-V** slurry. However, a further increase in KB loading (300 g/L) causes an increase in R_{ct} or poor charge transfer in the slurry, which could be ascribed to the aggregation of KB particles. Therefore, a KB loading of 240 g/L was employed for subsequent studies.

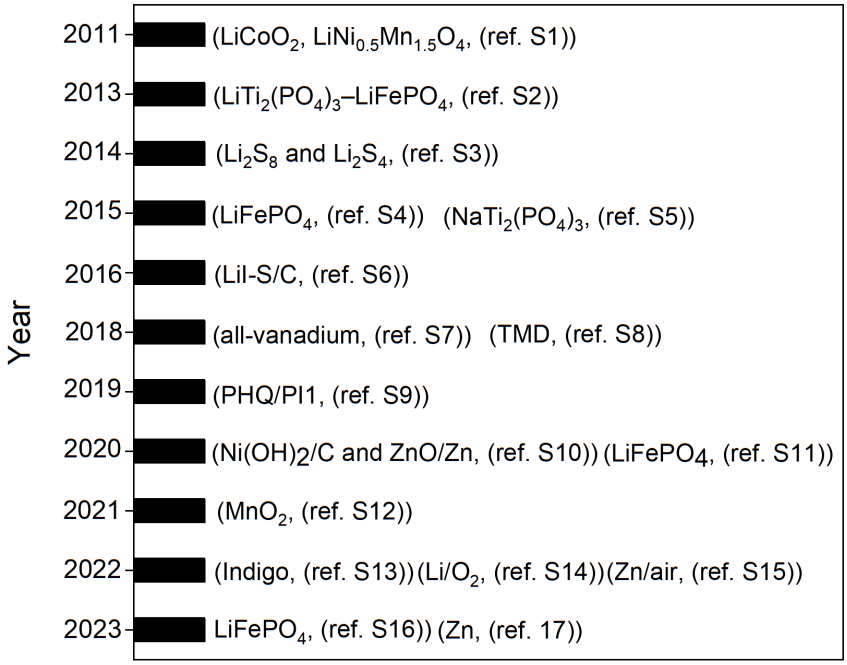

Fig. S1. Reported slurry-based flow battery using inorganic redox materials (ref. S1-17).

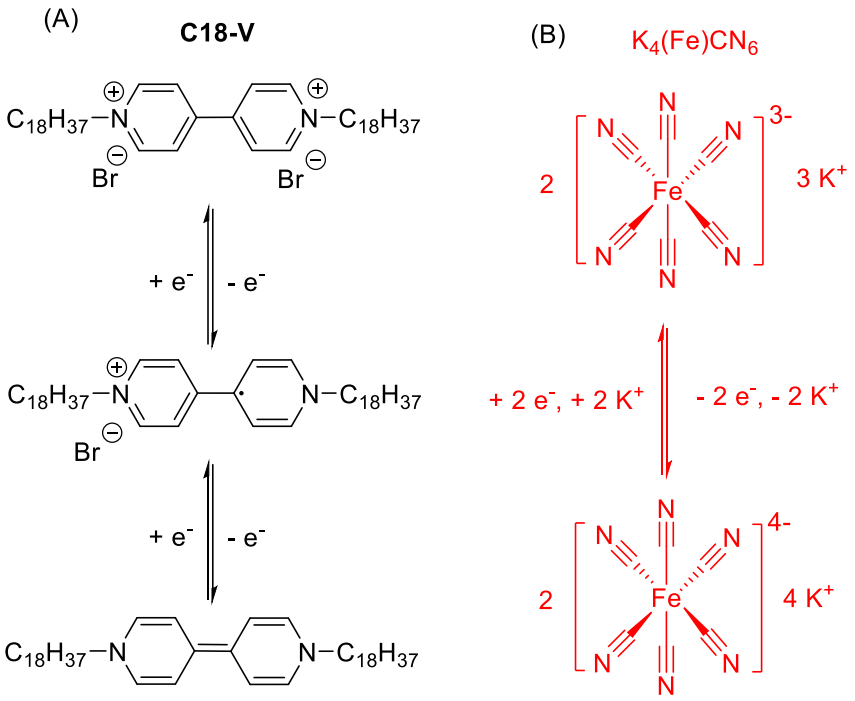

Fig. S2. Redox reactions of **C18-V** and $K_4Fe(CN)_6$.

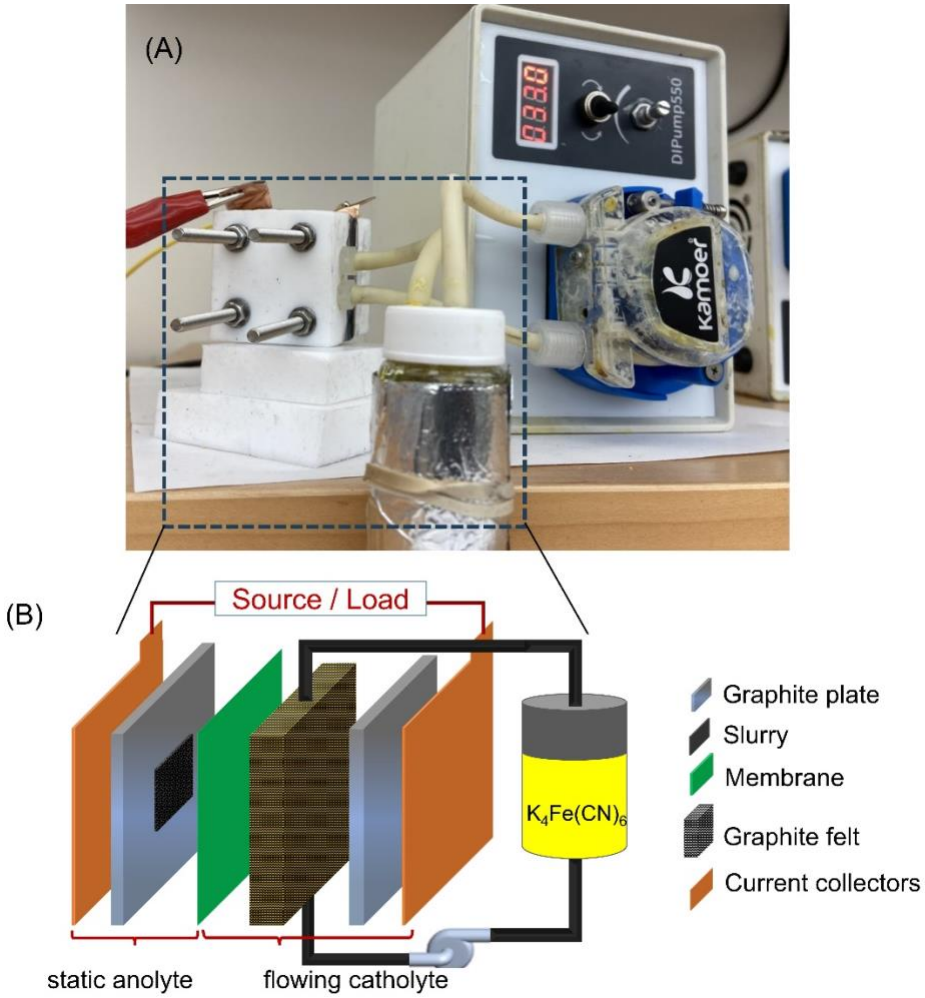

Fig. S3. (A) Digital photograph and (B) schematic diagram of **C18-V**||$K_4Fe(CN)_6$ static slurry battery setup.

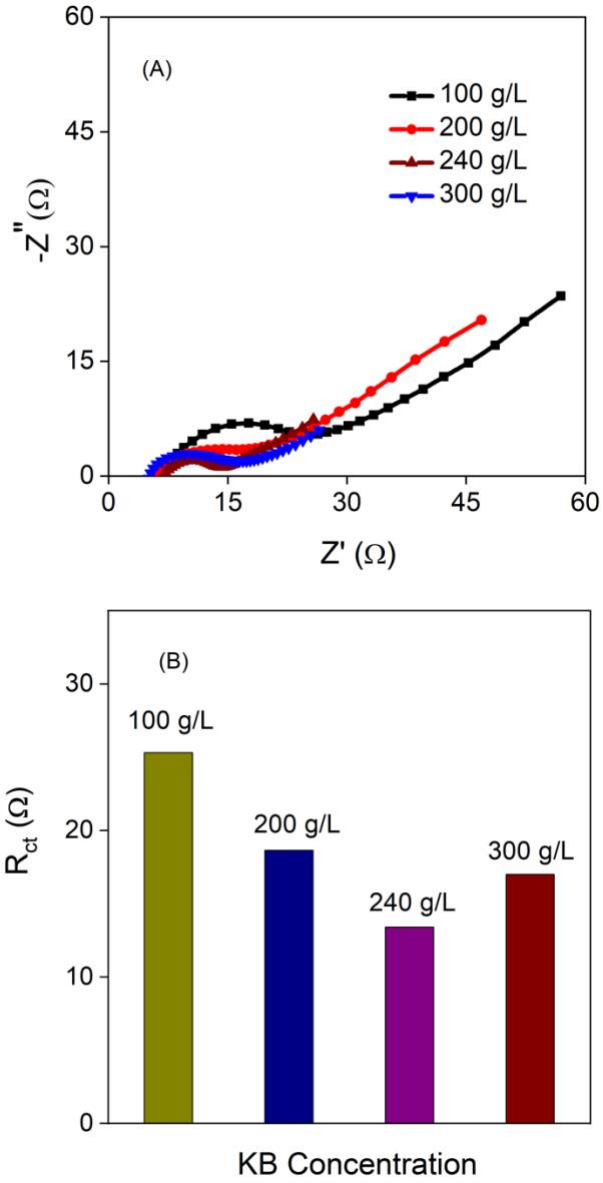

Fig. S4. (A) Electrochemical impedance spectroscopy analysis of **C18-V** slurry at different concentrations of KB. (B) Variation in charge transfer resistance (Rct) at different concentrations of KB in **C18-V** slurry.

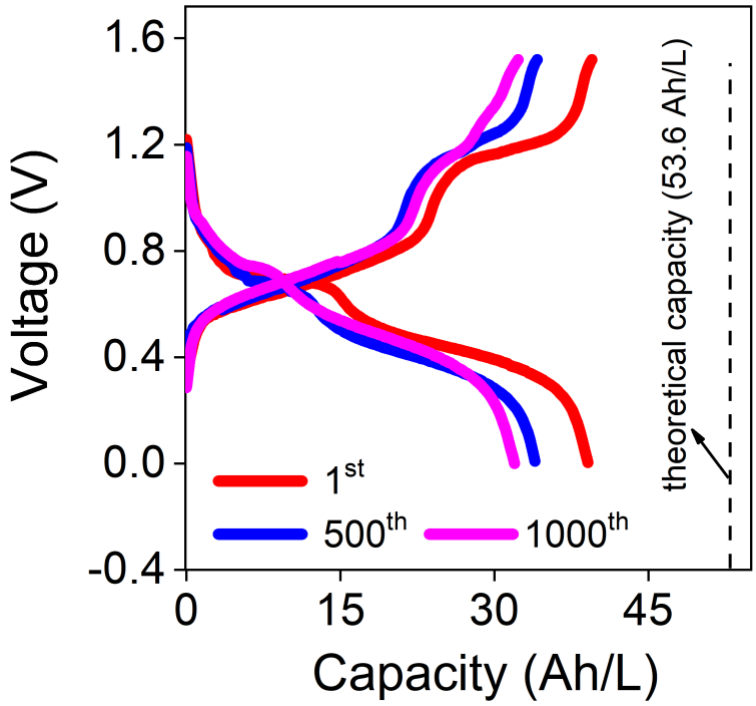

Fig. S5. Charge/discharge profiles of 1.0 M **C18-V**||$K_4Fe(CN)_6$ static slurry battery for the 1st, 500th, and 1000th cycles.

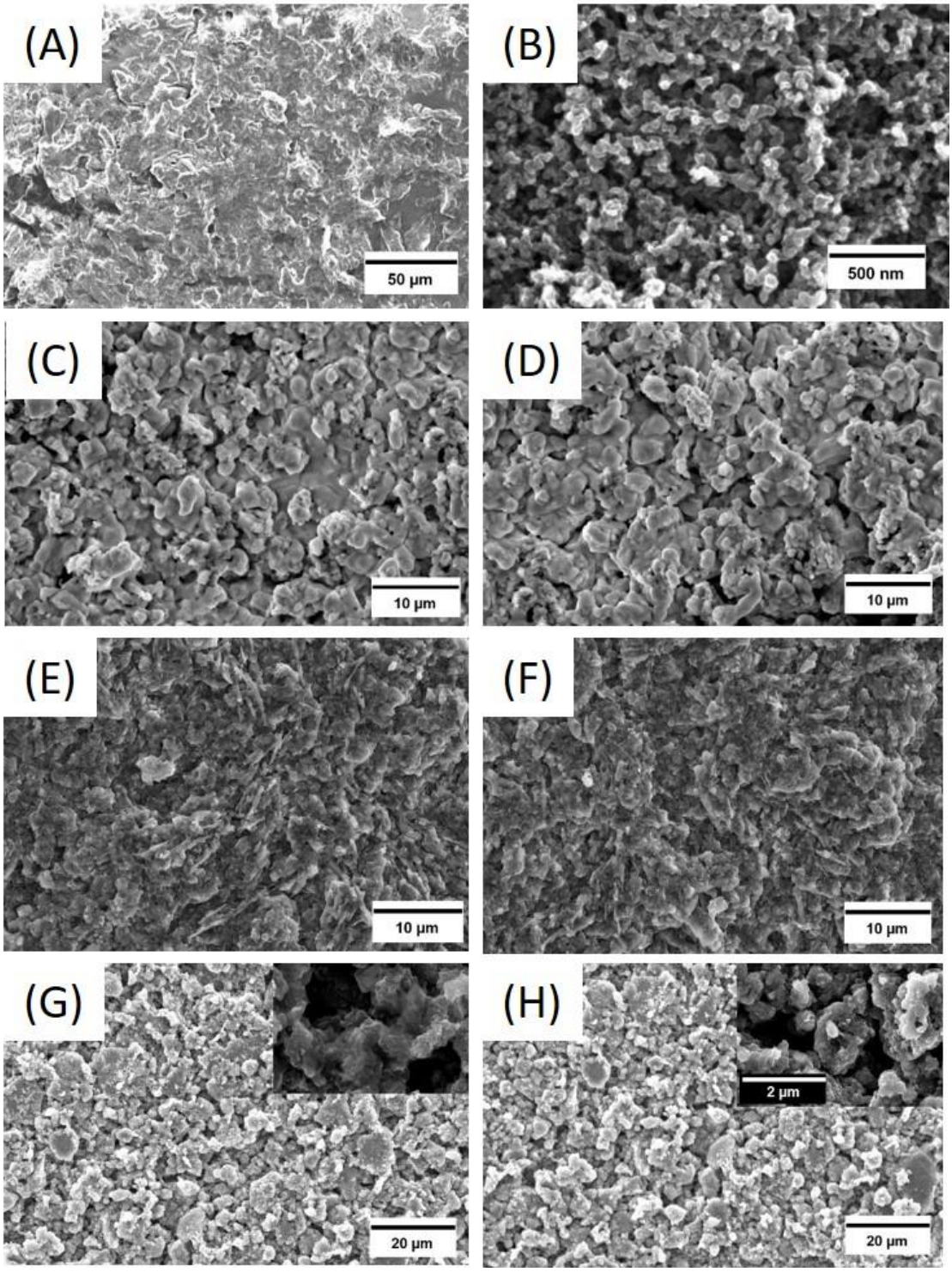

Fig. S6. Scanning electron microscopy morphology of (A) pure **C18-V**, (B) KB, 0.8 M **C18-V** slurry (C) before and (D) after 1000 charge/discharge cycles, 1.0 M **C18-V** slurry (E) before and (F) after 1000 charge/discharge cycles, and 1.15 M **C18-V** slurry (G) before and (H) after 1000 charge/discharge cycles.

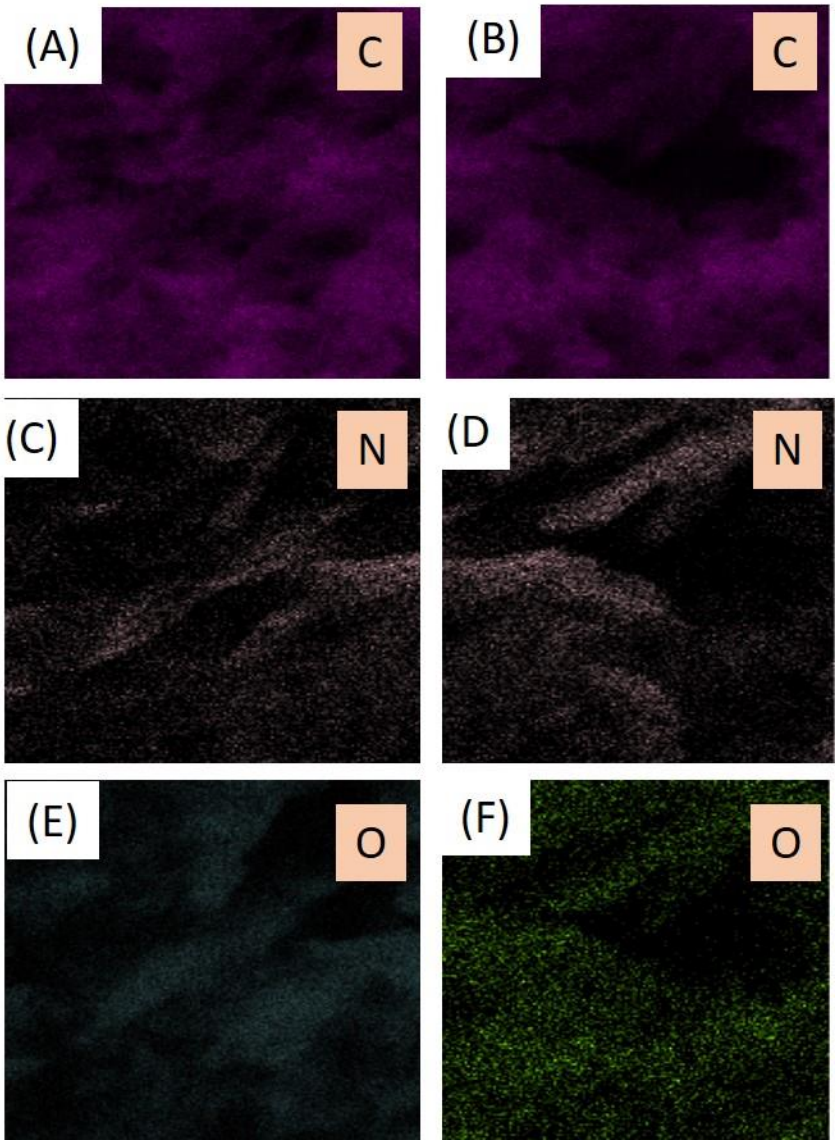

Fig. S7. Energy dispersive spectroscopy micrographs showing the distribution of elements in 1.0 M **C18-V** slurry. C element distribution (A) before cycling and (B) after 1000 charge/discharge cycles. N element distribution (C) before cycling and (D) after 1000 charge/discharge cycles. O element distribution (E) before cycling and (F) after 1000 charge/discharge cycles.

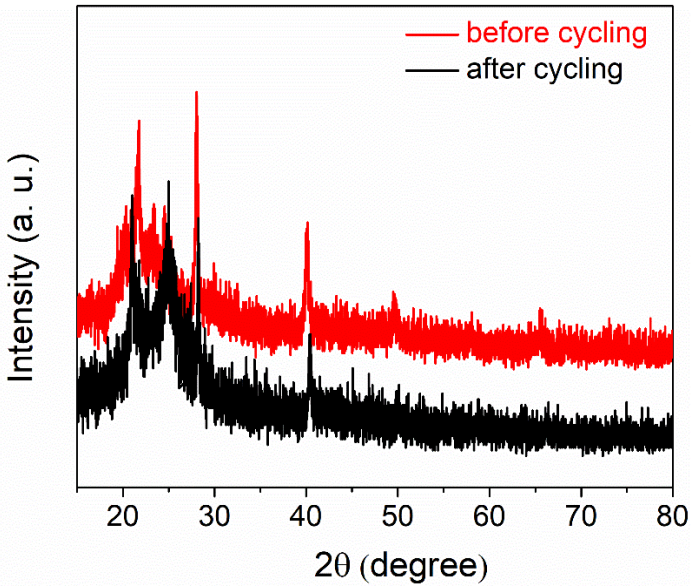

Fig. S8. X-ray diffraction patterns of 1.0 M **C18-V**slurry before and after 1000 charge/discharge cycles.

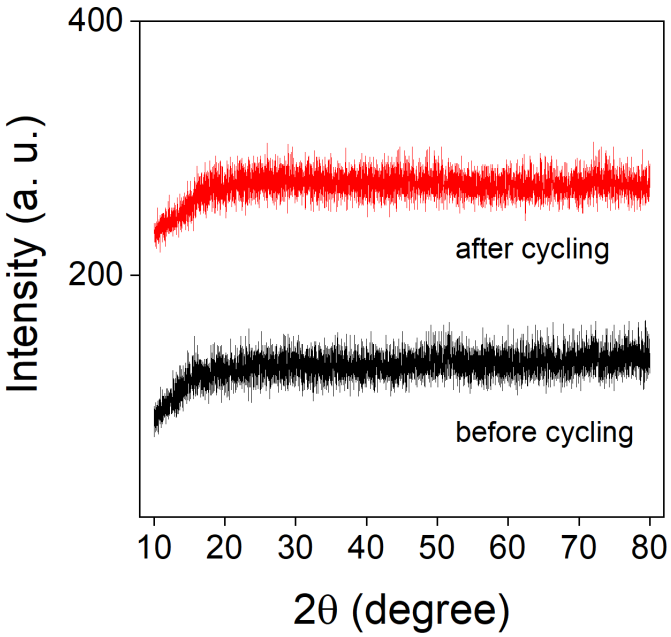

Fig. S9. X-ray diffraction pattern of the pre- and post-cycled battery membrane.

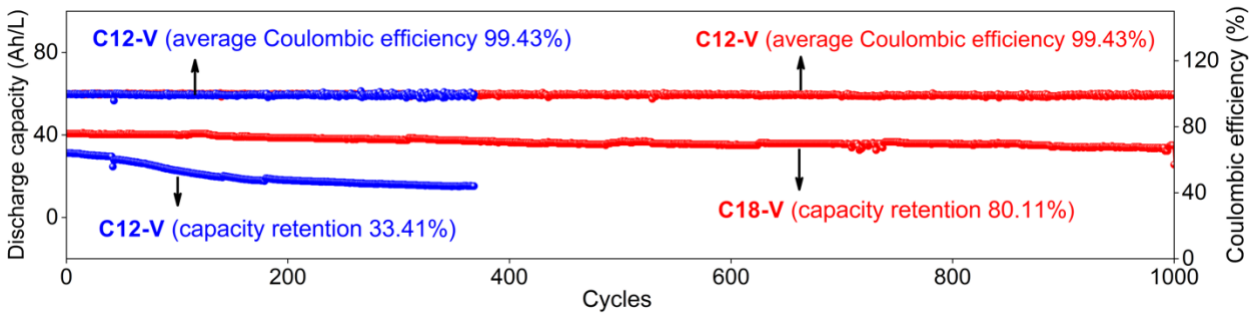

Fig. S10. Long-term cycling comparison of 1.0 M **C18-V**||$K_4Fe(CN)_6$ and 1.0 M **C12-V**||$K_4Fe(CN)_6$ slurry battery.

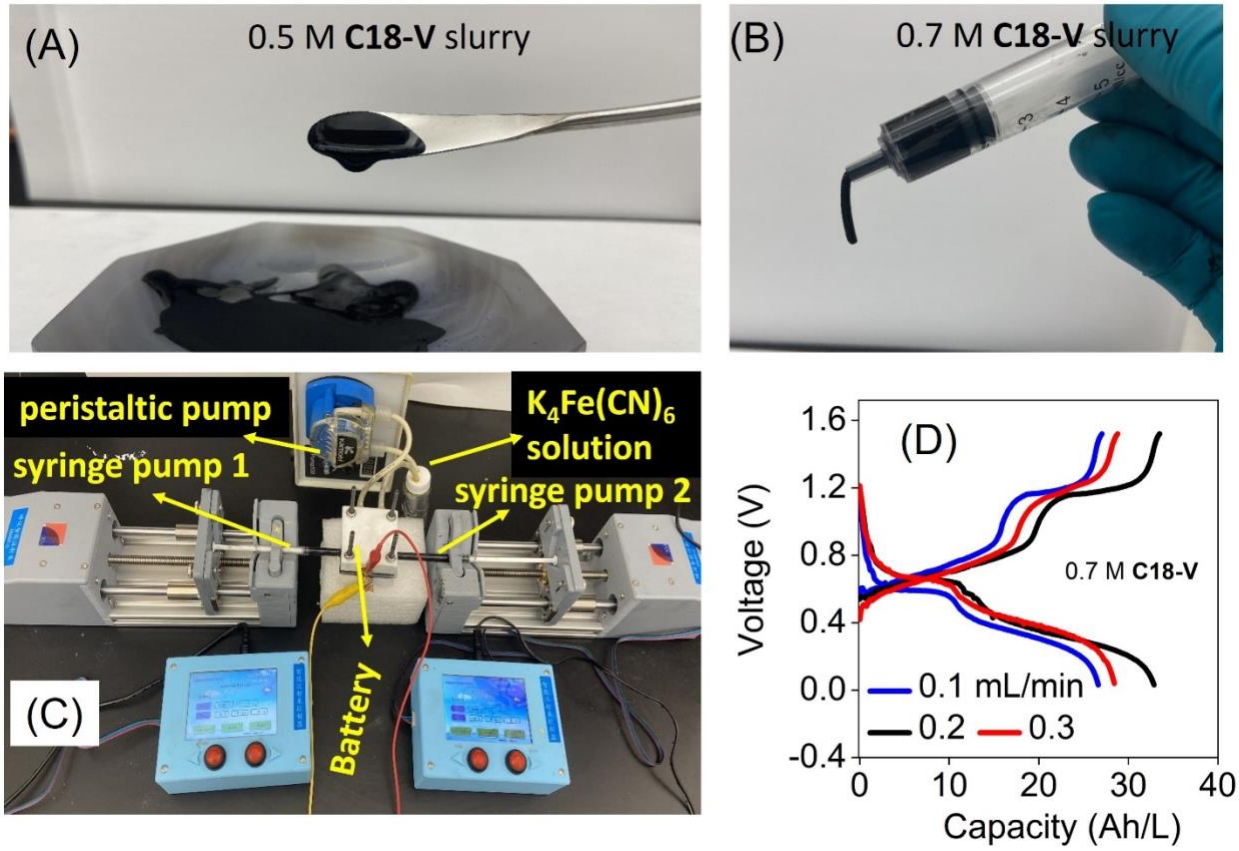

Fig. 11. Photographs of (A) 0.5 M **C18-V** slurry, (B) 0.7 M **C18-V** slurries, and (C) setup for slurry flow battery using two syringe pumps to flow the aqueous slurry. (D) Flow rate optimization for 0.7 M **C18-V**||$K_4Fe(CN)_6$ slurry flow battery for a given current density of 10 mA/cm^2.

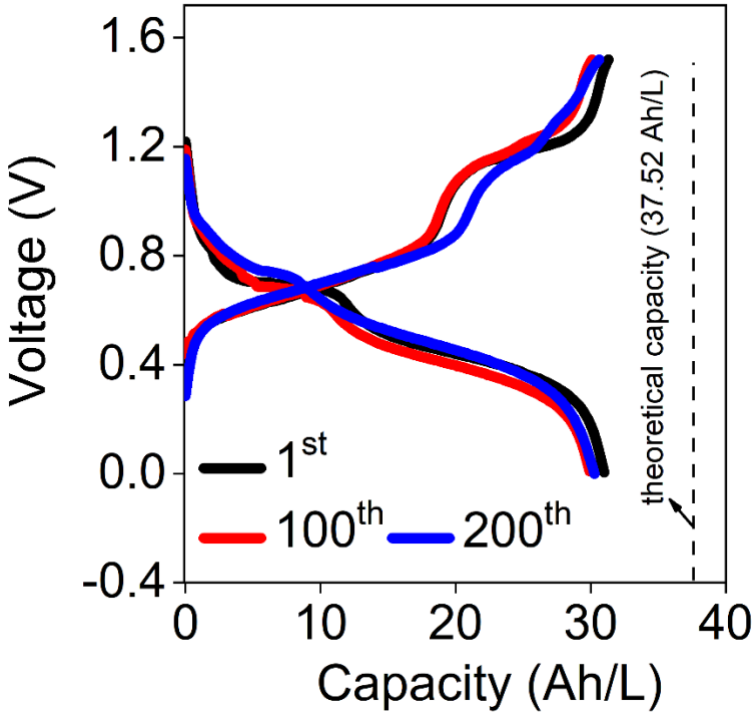

Fig. S12. Charge/discharge profiles of 0.7 M **C18-V**||$K_4Fe(CN)_6$ flow slurry battery for the 1st, 100th, and 200th cycles.

Table S1. Performance comparison of **C18-V**||$K_4Fe(CN)_6$ slurry battery with other batteries utilizing viologen as anolyte.

	Anolyte		Anolyte conc. (M)	Membrane	Capacity (Ah/L)	Discharge energy density (Wh/L)	Current density (mA/cm^2)	Cycle life (No.)	Coulombic efficiency (%)	Capacity retention		Ref.
										total (%)	per day (%)	
1	**C18-V** in 1 M KCl	static	1.0	Fumasep, CEM	40.6	29.2	10	1000	99.56	80.1	99.39	This Work
		static	0.8	Fumasep, CEM[a]	31.2	22.5	10	1000	99.73	82.3	99.34	
		flow	0.7	Fumasep, CEM	32.1	23.1	15	200	99.47	96.2	99.77	
		flow	0.5	Fumasep, CEM	23.2	16.7	15	200	99.83	97.1	99.73	
2	$(2HO\text{-}V)Br_2$ in 2 M NaCl		0.5	Porous polyolefin	25	14.2	20	100	98	-	-	S18
3	$[MV]Br_2$ in 2.0 M NaCl		0.5	Daramic	10	7.1	40	100	98	100	-	S19
4	$(SPr)_2V$ in 2.0 M KCl		0.5	Nafion 212, CEM	9	7.2	60	300	99	94	-	S19
5	$(SPr)_2V$ in 2.0 M KCl		0.5	Selemion, CEM	12	10.2	60	100	99	99	-	S19
6	MVI_2 in 1M NaCl		0.05	Astom, AEM	12	0.5	2	450	99	99	-	S20
7	$[(NPr)_2TTz]Cl_4$ in 2M NaCl		0.1	Selemion AEM	4	5.2	40	300	98	90	-	S21

8	$(ATBPy)Cl_4$	1.0	Selemion DSV, AEM	23	10.2	60	100	98	99	99.34	S22
9	MV in 1.5 M NaCl	0.5	Fumasep FAA-3-50, AEM	4.5	3.5	5	2500	97	16	-	S23
10	MV in water	2.0	Fumasep FAA-3-PE-30, AEM	40	48	80	100	89	93	-	S24
11	$(SO_3)V(OH)Br$ in Sat. NaCl	0.25	Selemion AME-115, AEM	13	17	30	200	99	75	-	S25
12	$(Me)(NPr)V]Cl_3$ in NaCl	0.25	Selemion AME-115, AEM	12	14.5	60	50	99	84	-	S26
13	$(NPr)_2V]Br_4$ in NaCl	0.5	Selemion AME-115, AEM	11	13.2	60	100	99	98	-	S26
14	$(NPr)_2V$ in	0.5	Selemion AMV, AEM	~9	11.3	60	500	99	97	-	S27
15	BPP−Vi in 1 M KCl	1.0	Fumasep E620(K), CEM	~26	23.4	40	280	99	99	99.98	S28
16	$[PyrPV]Cl_4$ in 2.0 m NaCl	0.25	Selemion DSV, AEM	11	17	40	1000	100	45	-	S29
17	R-Vi in 1 M KCl	0.1	Nafion 212, CEM	~3	2.7	50	3200	99	69	98.52	S30

18	S-Vi in 1 M KCl	0.1	Nafion 212, CEM	~2	1.6	50	1000	99	64	98.35	S30
19	MVTFSI	0.1	Daramic 175	4.2	4.6	30	100	96	93	-	S31
20	EV in 1 M NaBr	1.0	Selemion AMV, AEM	21.5	20.7	10	850	99	98	99.99	S32

[a]CEM: cation exchange membrane; AEM: anion exchange membrane.

References

S1. M. Duduta, B. Ho, V. C. Wood, P. Limthongkul, V. E. Brunini, W. C. Carter and Y. M. Chiang, *Adv. Energy Mater.*, 2011, **1**, 511–516.

S2. Z. Li, K. C. Smith, Y. Dong, N. Baram, F. Y. Fan, J. Xie, P. Limthongkul, W. C. Carter and Y. M. Chiang, *Phys. Chem. Chem. Phys.*, 2013, **15**, 15833–15839.

S3. F. Y. Fan, W. H. Woodford, Z. Li, N. Baram, K. C. Smith, A. Helal, G. H. McKinley, W. C. Carter and Y. M. Chiang, *Nano Lett*, 2014, **14**, 2210–2218.

S4. T. S. Wei, F. Y. Fan, A. Helal, K. C. Smith, G. H. McKinley, Y. M. Chiang and J. A. Lewis, *Adv. Energy Mater.*, 2015, **5**, 1500535.

S5. E. Ventosa, D. Buchholz, S. Klink, C. Flox, L. G. Chagas, C. Vaalma, W. Schuhmann, S. Passerini and J. R. Morante, *Chem. Commun.*, 2015, **51**, 7298–7301.

S6. H. Chen and Y. C. Lu, *Adv. Energy Mater.*, 2016, **6**, 1502183.

S7. K. Percin, A. Rommerskirchen, R. Sengpiel, Y. Gendel and M. Wessling, *J. Power Sources*, 2018, **379**, 228–233.

S8. C. Wang, Q. Lai, P. Xu, X. Li and H. Zhang, *Chin. Chem. Lett.*, 2018, **29**, 716-718.

S9. W. Yan, C. Wang, J. Tian, G. Zhu, L. Ma, Y. Wang, R. Chen, Y. Hu, L. Wang, T. Chen, J. Ma and Z. Jin, *Nat. Commun.*, 2019, **10**, 2513.

S10. M. Chen, L. Liu, P. Zhang and H. Chen, *RSC Adv.*, 2021, **11**, 24429–24435.

S11. N. Aguilo-Aguayo, D. Hubmann, F. U. Khan, S. Arzbacher and T. Bechtold, *Sci. Rep.*, 2020, **10**, 5565.

S12. T. M. Narayanan, Y. G. Zhu, E. Gençer, G. McKinley and Y. Shao-Horn, *Joule*, 2021, **5**, 2934–2954.

S13. X. Wang, J. Chai, S. Zhang, B. Chen, A. Chaturvedi, G. Cui and J. Jiang, *ACS Energy Lett.*, 2022, **7**, 1178–1186.

S14. F. Soavi, A. Brilloni, F. De Giorgio and F. Poli, *Curr. Opin. Chem. Eng.*, 2022, **37**.

S15. D. Perez-Antolin, W. Schuhmann, J. Palma and E. Ventosa, *J. Power Sources*, 2022, **536**.

S16. S. Cheng, Y. Hu, L. Jiang, H. Dang, Y. Ding, Q. Duan, H. Xiao, J. Sun and Q. Wang, *Fire Technol.*, 2022, **59**, 1181–1197.

S17. Z. Yang, Q. Zhang, W. Li, C. Xie, T. Wu, C. Hu, Y. Tang and H. Wang, *Angew. Chem. Int. Ed.*, 2023, **62**, e202215306.

S18. W. Liu, Y. Liu, H. Zhang, C. Xie, L. Shi, Y. G. Zhou and X. Li, *Chem. Commun.*, 2019, **55**, 4801–4804.

S19. C. DeBruler, B. Hu, J. Moss, J. Luo and T. L. Liu, *ACS Energy Lett.*, 2018, **3**, 663–668.

S20. S. Liu, M. Zhou, T. Ma, J. Liu, Q. Zhang, Z. Tao and J. Liang, *Chin. Chem. Lett.*, 2020, **31**, 1690–1693.

S21. J. Luo, B. Hu, C. Debruler and T. L. Liu, *Angew. Chem.*, 2018, **130**, 237–241.

S22. B. Hu, H. Fan, H. Li, M. Ravivarma and J. Song, *Adv. Funct. Mater.*, 2021, **31**, 2102734.

S23. T. Hagemann, J. Winsberg, M. Grube, I. Nischang, T. Janoschka, N. Martin, M. D. Hager and U. S. Schubert, *J. Power Sources*, 2018, **378**, 546–554.

S24. T. Janoschka, N. Martin, M. D. Hager and U. S. Schubert, *Angew. Chem. Int. Ed.*, 2016, **55**, 14427–14430.

S25. H. Wang, D. Li, J. Xu, Y. Wu, Y. Cui and L. Chen, *J. Power Sources*, 2021, **492**, 229659.

S26. C. DeBruler, B. Hu, J. Moss, X. Liu, J. Luo, Y. Sun and T. L. Liu, *Chem*, 2017, **3**, 961–978.

S27. B. Hu, Y. Tang, J. Luo, G. Grove, Y. Guo and T. L. Liu, *Chem. Commun.*, 2018, **54**, 6871–6874.
S28. S. Jin, E. M. Fell, L. Vina-Lopez, Y. Jing, P. W. Michalak, R. G. Gordon and M. J. Aziz, *Adv. Energy Mater.*, 2020, **10**, 2000100.
S29. M. Pan, L. Gao, J. Liang, P. Zhang, S. Lu, Y. Lu, J. Ma and Z. Jin, *Adv. Energy Mater.*, 2022, **12**, 2103478.
S30. H. Li, H. Fan, B. Hu, L. Hu, G. Chang and J. Song, *Angew. Chem. Int. Ed.*, 2021, **60**, 26971–26977.
S31. B. Hu and T. L. Liu, *J. Energy Chem.*, 2018, **27**, 1326–1332.
S32. L. Liu, Y. Yao, Z. Wang and Y. C. Lu, *Nano Energy*, 2021, **84**, 105897.